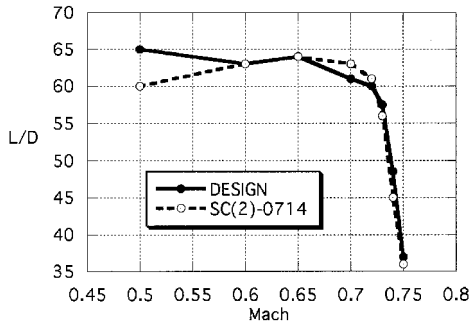

Fig. 3 Comparison of aerodynamic performance.

To compare relative aerodynamic performance, *L/D* is plotted at various Mach numbers in Fig. 3. From the plots, the present design is found to perform better than SC(2)-0714, except at Mach numbers of 0.7 and 0.72 (slightly lower than the design point of 0.73). Although only a straight base is considered for the airfoil closure here, Ref. 8 suggests that the inclusion of cavity at the base might further reduce the drag.

References

[1]Obayashi, S., and Takanashi, S., "Genetic Optimization of Target Pressure Distributions for Inverse Design Methods," *AIAA Journal*, Vol. 34, No. 5, 1996, pp. 881–886.

[2]Henne, P. A., "Innovation with Computational Aerodynamics: The Divergent Trailing-Edge Airfoil," *Applied Computational Aerodynamics*, edited by P. A. Henne, Vol. 125, Progress in Astronautics and Aeronautics, AIAA, Washington, DC, 1990, pp. 221–262.

[3]Stanaway, S. K., McCroskey, W. J., and Kroo, I. M., "Navier-Stokes Analysis of Blunt Trailing Edge Airfoils," AIAA Paper 92-0024, Jan. 1992.

[4]Monsen, E., and Rudnik, R., "Investigation of the Blunt Trailing Edge Problem for Supercritical Airfoils," AIAA Paper 95-0089, Jan. 1995.

[5]Thompson, B. E., and Lotz, R. D., "Divergent-Trailing-Edge Airfoil Flow," *Journal of Aircraft*, Vol. 33, No. 5, 1996, pp. 950–955.

[6]Obayashi, S., Jeong, S., and Matsuo, Y., "Inverse Optimization Method for Blunt-Trailing-Edge Airfoils," *Proceedings of the 15th International Conference on Numerical Methods in Fluid Dynamics* (Monterey, CA), Springer–Verlag, Berlin, 1997, pp. 206–211.

[7]Takanashi, S., "Iterative Three-Dimensional Transonic Wing Design Using Integral Equations," *Journal of Aircraft*, Vol. 22, No. 8, 1985, pp. 655–660.

[8]Harris, C. D., "NASA Supercritical Airfoils — A Matrix of Family-Related Airfoils," NASA TP-2969, March 1990.

Induced Drag Calculation by Numerical Lifting Surface Method

Masami Ichikawa* and Akira Matsuda*
Okayama Prefectural University, Soja, Okayama 719-11, Japan

Nomenclature

b = wingspan length
C_{Di} = total induced drag coefficient
C_L = total lift coefficient
C_T = total thrust coefficient
c = local chord length
c_{di} = sectional induced drag coefficient
c_l = sectional lift coefficient
c_t = sectional thrust coefficient
S = wing planform area
T_n = Chebychev polynomial of degree n of the first kind
α = angle of attack
ΔC_p = difference between lower and upper pressure coefficients

Superscripts
F = far-field method
N = near-field method

Received Aug. 13, 1996; revision received Nov. 15, 1996; accepted for publication Nov. 30, 1996.

*Assistant Professor, Department of System Engineering, Faculty of Computer Science and System Engineering, Kuboki 111.

Introduction

THE calculation of induced drag is one of the difficult problems for the discrete numerical lifting surface methods because it requires a very accurate computation of the lift distribution. Since the numerical accuracy near the leading edge of the conventional vortex lattice method (VLM) is not adequate, VLM cannot predict the near-field induced drag as precisely as that of the far field. There are several works[1,2] to improve the accuracy near the leading edge of the VLM solution. The quasi-vortex-lattice method (QVLM) by Lan[3] appears to be the only one among those methods that has succeeded in obtaining adequate results for two calculation methods of the induced drag. Most of the numerical lifting surface methods including QVLM have only investigated the agreement of the near- and far-field induced drags because it has been taken as the performance indicator of the numerical methods, but they have not addressed the accuracy of the predicted values sufficiently. In Ref. 4, the present authors have shown the analytical solutions of the induced drag in terms of the near and far fields for the elliptic wing in steady incompressible flow using Kida's method.[5] This Note investigates, through the analytical results in Ref. 4, the performance for the induced drag calculation of QVLM and box-in-strip method (BISM)[6] developed by one of the present authors.

Method

The computational method of the induced drag by QVLM is addressed in Ref. 3, whereas that by BISM must be formulated and incorporated into a computer program. First, the near-field induced drag calculation is considered.

Since BISM utilizes the Stark's quadrature formula[7] for evaluating the Cauchy singularity in the lifting surface integral equation, it calculates the values of ΔC_p at the points (x_i, y) expressed by the cosine law distribution:

$$x_i = x_m + (c/2)\cos\beta_i, \qquad i = 1, \ldots, n \tag{1}$$

where x_m denotes the x coordinate of the midpoint on the local chord, $\beta_i = 2i\pi/(2n + 1)$, and n is the total number of chordwise collocation points. The spanwise coordinate y of the collocation point can be determined arbitrarily and will not be specified here. It is found that $\cos\beta_i$ are the zero points of function $G_n(\xi)$ defined by $[T_{n+1}(\xi) - T_n(\xi)]/(1 - \xi)$, and it is also shown that $G_n(\xi)$ is the orthogonal polynomial of degree n on the interval $[-1, 1]$ with respect to the weighting function $[(1 - \xi)/(1 + \xi)]^{1/2}$, which expresses the singularity at the leading and trailing edges in the thin wing theory. Using the Lagrangian interpolation formula, the chordwise distribution of ΔC_p can be approximated by the following equation:

$$\Delta C_p(x, y) = \sum_{i=1}^{n} g_i(\xi)\Delta C_p(x_i, y) \tag{2}$$

Table 1 Comparison of the total induced drag coefficient for circular and elliptic wings in steady incompressible flow

	a) Circular wing (aspect ratio = $4/\pi$)			b) Elliptic wing (aspect ratio = 10)		
Method	C_L	$C_{D_i}^F$	$C_{D_i}^N$	C_L	$C_{D_i}^F$	$C_{D_i}^N$
BISM ($m = 120$, $n = 5$)	1.790	0.801	0.801	5.062	0.816	0.811
QVLM ($m = 120$, $n = 5$)	1.790	0.801	0.796	5.062	0.815	0.812
Analytical (Ref. 4)	1.790	0.801	0.801	5.062	0.816	0.816

where ξ is the nondimensional coordinate defined by $2(x - x_m)/c$, and the functions g_i are defined by

$$g_i(\xi) = \sqrt{\frac{1-\xi}{1+\xi}}\sqrt{\frac{1+\xi_i}{1-\xi_i}}\frac{G_n(\xi)}{(\xi-\xi_i)G_n'(\xi_i)} \tag{3}$$

in which $\xi_i = \cos\beta_i$ and the prime denotes the differentiation with respect to ξ. Use of Eqs. (2) and (3) yields the following result:

$$\lim_{x\to x_l}\sqrt{x-x_l}\Delta C_p(x,y) = \sqrt{\frac{c}{2}}\lim_{\xi\to -1}\sqrt{1+\xi}\Delta C_p(x,y)$$

$$= (-1)^n\sqrt{c}\sum_{i=1}^{n}\frac{\Delta C_p(x_i,y)}{\sqrt{1-\xi_i^2}\,G_n'(\xi_i)} \tag{4}$$

where x_l is the x coordinate of the local leading edge. Hence, the sectional leading-edge thrust coefficient can be estimated by

$$c_t(y) = \frac{\pi\sqrt{1-M_\infty^2\cos^2\Lambda_l}}{8\cos\Lambda_l}\left[\sum_{i=1}^{n}\frac{\Delta C_p(x_i,y)}{\sqrt{1-\xi_i^2}G_n'(\xi_i)}\right]^2 \tag{5}$$

where M_∞ is the freestream Mach number and Λ_l is the local leading-edge sweep angle. This formula includes only the points in the strip to be considered, and is obviously different from the formula in Ref. 3. Now the sectional induced drag coefficient is given by $c_{d_i}^N = c_l\alpha - c_t$ and the total induced drag coefficient by $C_{D_i}^N = C_L\alpha - C_T$.

The far-field induced drag is given by

$$C_{D_i}^F = \frac{1}{S}\int_{-b/2}^{+b/2} c_l c\alpha_i\,dy \tag{6}$$

where α_i is the induced angle of attack given by

$$\alpha_i(y) = -\frac{1}{8\pi}\int_{-b/2}^{+b/2}\frac{c_l c}{(y-\eta)^2}\,d\eta \tag{7}$$

In evaluating Eqs. (6) and (7), the following interpolation formula may be used for $c_l c$:

$$c_l c = \frac{2}{m+1}\sum_{j=1}^{m}(c_l c)_j\sum_{k=1}^{m}\sin k\phi_j\sin k\phi \tag{8}$$

where m is the total number of spanwise strips and

$$\phi_j = j\pi/(m+1), \qquad j = 1,\ldots,m \tag{9}$$

Then, Eq. (7) can be integrated resulting in

$$\alpha_i = \frac{1}{2b(m+1)\sin\theta}\sum_{j=1}^{m}(c_l c)_j\sum_{k=1}^{m}k\sin k\phi_j\sin k\theta \tag{10}$$

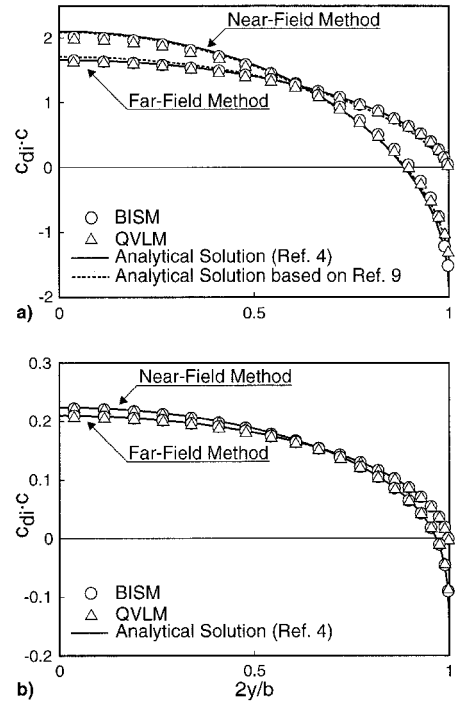

Fig. 1 Comparison of computed sectional induced drag distributions with the analytical solutions for a) circular and b) elliptic wings in steady incompressible flow.

with $y = -(b/2)\cos\theta$ and the following relation:

$$\int_0^\pi\frac{\sin\phi\sin k\phi}{(\cos\phi-\cos\theta)^2}\,d\phi = \pi k\frac{\sin k\theta}{\sin\theta}, \qquad k = 1,2,\ldots \tag{11}$$

Once α_i is obtained, Eq. (6) can be integrated easily to give

$$C_{D_i}^F = \frac{\pi}{4(m+1)^2 S}\sum_{k=1}^{m}k\left[\sum_{j=1}^{m}\sin(k\phi_j)(c_l c)_j\right]^2 \tag{12}$$

Equation (12) is substantially identical with the corresponding equation in Ref. 8 obtained by the midpoint trapezoidal rule and the theory of Chebychev polynomials. Hence, the sectional induced drag coefficient of the far-field method can be computed by $c_{d_i}^F = c_l\alpha_i$.

Numerical Results

In numerical calculations, α is assumed to be 1 rad and the flow is incompressible. Table 1 shows comparison studies of the total induced drags for the circular and elliptic wings with the theoretical values. For the far-field case, the computed results by two numerical methods agree well with the theoretical results. For the near-field case, the accuracy of numerical methods is not as good as that in the far-field case; QVLM gives fairly close values to the theoretical results, whereas the accuracy of BISM is excellent in the case of the circular wing but is slightly inferior to that of QVLM in the case of the

elliptic wing. Figures 1a and 1b show the spanwise distributions of the sectional induced drags for the cases of Table 1. The dashed lines in Fig. 1a are analytical results based on Hauptman and Miloh's method,[9] which produces the closed solution of the linearized lifting surface problem for the thin elliptic wings in steady incompressible potential flow. As can be seen from these figures, both of two numerical methods not only agree well with each other in the far- and near-field cases, but almost agree with the theoretical results in Ref. 4. It is noticed that neither of the numerical far-field induced drag distributions for the circular wing follow the analytical result based on Hauptman and Miloh's method.[9] Actually, when applying their method to the procedure in Ref. 4, the total induced drag coefficients of the circular wing with the angle of attack being 1 rad are

$$C_{\mathrm{Di}}^{N} = C_L^2/4 = 0.80169\ldots$$

$$C_{\mathrm{Di}}^{F} = \frac{C_L^2}{16}\sum_{j,k=0}^{\infty}\frac{1}{(2j+1)(2k+1)}\left(\frac{2}{2j-2k+1} - \frac{1}{j+k+2} - \frac{2}{2j-2k-1} + \frac{1}{j+k+1}\right) = 0.80313\ldots$$

where C_L should be taken as the value predicted by their method, $32/(8+\pi^2)$. The two values coincide with each other only to the second decimal place, whereas the corresponding values in Table 1a do so to three places. This result indicates that their method may be approximate because it does not satisfy the fact that the near- and the far-field induced drags should agree in the thin wing theory.

Conclusions

This Note has investigated the accuracy in the induced drag calculation using the discrete numerical lifting surface methods, QVLM and BISM. The formula presented for estimating the leading-edge thrust distribution by the latter numerical method has proven to be useful, which was different from that of QVLM. Both numerical methods have given very close results with respect to both near- and far-field calculations of the induced drag. Moreover, they have agreed very well with the theoretical results presented in Ref. 4 rather than those based on Hauptman and Miloh's method.[9]

References

[1]Kalman, T. P., Giesing, J. P., and Rodden, W. P., "Spanwise Distribution of Induced Drag in Subsonic Flow by the Vortex Lattice Method," *Journal of Aircraft*, Vol. 7, No. 2, 1970, pp. 574–576.

[2]Lan, C. T., and Roskam, J., "Leading-Edge Force Features of the Aerodynamic Finite Element Method," *Journal of Aircraft*, Vol. 9, No. 12, 1972, pp. 864–867.

[3]Lan, C. E., "A Quasi-Vortex-Lattice Method in Thin Wing Theory," *Journal of Aircraft*, Vol. 11, No. 9, 1974, pp. 518–527.

[4]Ichikawa, M., "Analytical Expression of Induced Drag for a Finite Elliptic Wing," *Journal of Aircraft*, Vol. 33, No. 3, 1996, pp. 632–634.

[5]Kida, T., "A Theoretical Treatment of Lifting Surface Theory of an Elliptic Wing," *Zeitschrift fur Angewandte Mathematik und Mechanik*, Vol. 60, Dec. 1980, pp. 645–651.

[6]Ando, S., and Ichikawa, M., "A New Numerical Method of Subsonic Lifting Surfaces—BIS," *Transactions of the Japan Society for Aeronautical and Space Sciences*, Vol. 29, No. 84, 1986, pp. 101–118.

[7]Stark, V. J. E., "A Generalized Quadrature Formula for Cauchy Integrals," *AIAA Journal*, Vol. 9, No. 9, 1971, pp. 1854, 1855.

[8]DeJarnette, F. R., "Arrangement of Vortex Lattices on Subsonic Wings," *Vortex-Lattice Utilization*, NASA SP-405, N76-28180, Jan. 1976, pp. 301–323.

[9]Hauptman, A., and Miloh, T., "On the Exact Solution of the Linearized Lifting Surface Problem of an Elliptic Wing," *Quarterly Journal of Mechanics and Applied Mathematics*, Vol. 39, Pt. 1, 1986, pp. 41–66.

Application of Wagner Functions in Symmetrical Airfoil Design

N. Onur*
Gazi University, 06570 Maltepe, Ankara, Turkey

Introduction

A FAIR amount of experience in airfoil design for various applications has been gained over the years. This is because the aircraft industry needs to develop products for new applications with an increased efficiency for achieving better economic results. Today the airfoil design procedure is being computerized. The specification of airfoil geometry in a suitable functional form is quite useful when implementing a computer code. Different methods for the design of airfoil shapes have already been developed or are currently under investigation.[1–3]

The literature survey indicates that there is a need to look for and try new functions to represent airfoil geometry. The functional relationship used should be numerically well conditioned as well as be suitable to represent a wide class of airfoil shapes. It should also have computational efficiency. In this study, the slope of the airfoil is represented by a Fourier series expansion of the Wagner functions.[4] It was found that the representation of airfoil contour in terms of Wagner functions seems to meet the previously mentioned requirements. Studies with Wagner functions showed that a large class of airfoils can be adequately described by a small number of terms. The unknown coefficients in the series representation are obtained by the least-square method. Standard NACA and NASA NFL(1)-00115 airfoil data[5–7] were used to test the suitability of Wagner function representation of airfoil shapes. It was observed that the results were quite satisfactory.

Analysis

Consider a symmetrical thin airfoil. The airfoil is assumed to be at zero angle attack. The distance along the chord line measured from the leading edge is denoted by x. Suppose that the slope of airfoil can be represented as follows:

$$f'(x) = -A_0 + \sum_{n=0}^{\infty} A_n H_n(\phi) \tag{1}$$

where ϕ is related to x by $1 - 2x = \cos\phi$ and $f'(x)$ is the slope of the airfoil. The Wagner functions are given by

$$H_n(\phi) = \frac{2}{\pi}\frac{\cos[(n+1)\phi] + \cos(n\phi)}{\sin\phi} \tag{2}$$

Equation (1) is integrated to obtain the airfoil contour and it can be represented by

$$f(\theta) = A_0\left[\left(\frac{\phi + \sin\phi}{\pi}\right) - \sin^2\frac{\phi}{2}\right] + \frac{1}{\pi}\sum_{n=1}^{\infty}\left\{\frac{\sin[(n+1)\phi]}{n+1} + \frac{\sin(n\phi)}{n}\right\} \tag{3}$$

Standard airfoil shapes are used to test the suitability of Eq. (3) in representing airfoil contours.

Received Aug. 13, 1996; revision received Nov. 12, 1996; accepted for publication Nov. 18, 1996.

*Associate Professor, Faculty of Engineering and Architecture, Mechanical Engineering Department.